Energy & Environmental Science

Cite this: *Energy Environ. Sci.*, 2011, **4**, 2558

www.rsc.org/ees

PAPER

Carbon riveted microcapsule Pt/MWCNTs-TiO_2 catalyst prepared by *in situ* carbonized glucose with ultrahigh stability for proton exchange membrane fuel cell†

Zheng-Zhi Jiang,[ab] Zhen-Bo Wang,*[a] Yuan-Yuan Chu,[ab] Da-Ming Gu[b] and Ge-Ping Yin[a]

Received 24th January 2011, Accepted 15th April 2011
DOI: 10.1039/c1ee01091c

Pt/MWCNTs (Multi-walled carbon nanotubes, MWCNTs) and microcapsule Pt/MWCNTs-TiO_2 catalysts have been prepared by microwave-assisted polyol process (MAPP). Electrochemical results show that microcapsule Pt/MWCNTs-TiO_2 catalyst has higher activity and stability than Pt/MWCNTs due to more uniform dispersion and smaller size of Pt nanoparticles. Furthermore, carbon riveted microcapsule Pt/MWCNTs-TiO_2 catalyst has been designed and synthesized on the basis of *in situ* carbonization of glucose. The physical characteristics such as XRD, TEM, HRTEM, STEM, and XPS have indicated that the anatase TiO_2 indeed entered the inside of the MWCNTs and formed the microcapsule support of MWCNTs with TiO_2. The accelerated potential cycling tests (APCT) indicate that the carbon riveted microcapsule Pt/MWCNTs-TiO_2 catalyst with similar activity to microcapsule Pt/MWCNTs-TiO_2 and Pt/C possesses 7.5-times as high stability as that of Pt/C and has 3-times as long life-span as that of carbon riveted Pt/TiO_2-C reported in our previous work. The significantly enhanced stability for carbon riveted microcapsule Pt/MWCNTs-TiO_2 catalyst is assignable to: (1) the inherently excellent mechanical resistance and stability of anatase TiO_2 and MWCNTs in acidic and oxidative environments; (2) strong metal-support interaction between Pt nanoparticles and the microcapsule support; (3) the anchoring effect of the carbon layers formed during the carbon riveting process.

1. Introduction

Proton exchange membrane fuel cells (PEMFCs) are considered to be promising future power sources that are appropriate for stationary and mobile applications, with many advantages over other power sources.[1–3] However, the stability of Pt-based catalysts at both the anode and the cathode continue to stifle market entry.[4,5] So the development of a durable, low cost, highly active

[a]*School of Chemical Engineering and Technology, Harbin Institute of Technology, No.92 West-Da Zhi Street, Harbin, 150001, China. E-mail: wangzhenbo1008@yahoo.com.cn; Fax: +86-451-86418616; Tel: +86-451-86417853*
[b]*School of Science, Harbin Institute of Technology, No.92 West-Da Zhi Street, Harbin, 150001, China*

† Electronic supplementary information (ESI) available. See DOI: 10.1039/c1ee01091c

Broader context

Proton exchange membrane fuel cells (PEMFCs) have been attracting increasing interest all over the world because of their environmental friendliness, high energy density, low-temperature operation, fast start-up, and the possibility for automotive and portable electrical applications. However, the durability of Pt-based catalysts can still not fulfil the requirements of the commercialization of PEMFCs. Furthermore, the corrosion of carbon support in the catalysts is one of the main factors deteriorating the performances of PEMFCs during the long-term operation. Herein, microcapsule support of MWCNTs with anatase TiO_2 has been used as a novel catalyst support for PEMFCs and the microcapsule Pt/MWCNTs-TiO_2 catalyst has been synthesized by microwave-assisted polyol process (MAPP). The obtained microcapsule Pt/MWCNTs-TiO_2 showed higher activity and stability than Pt/C under the same conditions. Furthermore, a novel microcapsule Pt/MWCNTs-TiO_2 catalyst covered with carbon layers (denoted as carbon riveted microcapsule Pt/MWCNTs-TiO_2) based on *in situ* carbonization of glucose has been designed and synthesized. Experimental results show that carbon riveted microcapsule Pt/MWCNTs-TiO_2 catalyst exhibits much higher stability than that of Pt/C and that of carbon riveted Pt/TiO_2-C reported in our previous work. These findings indicate carbon riveted microcapsule Pt/MWCNTs-TiO_2 is one kind of potential catalyst to accelerate the commercialization process of PEMFCs.

electrocatalyst is one of the most critical challenges for the successful introduction of PEMFCs into the market.[2,6–8]

Carbon black[9–11] has been the most widely studied catalyst support for PEMFCs because of its large surface area, high electrical conductivity, and well-developed appropriate pore structure. Conclusions from previous reports[12–14] indicate that the corrosion of carbon black in the catalysts is one of the main factors affecting their performance and long-term durability.

Carbon nanotubes (CNTs), by virtue of their specific properties such as nanometre size, electronic properties, high surface area and nice corrosion resistance, have been receiving increased attention in recent years for their application in fuel cells as supports for catalysts.[15,16] Earlier studies have shown that CNTs are more corrosion resistant than carbon black in the working environment of fuel cells.[17,18] However, according to the state-of-the-art stability of Pt/CNTs, the requirements of the commercialization of PEMFCs still cannot be fulfilled.[6]

So far, TiO_2 and TiO_2-based composites[19–21] have attracted increasing attention as alternative catalyst supports due to excellent mechanical resistance and stability of TiO_2 in acidic and oxidative environments. Furthermore, over the past few years, CNTs have been combined with a variety of inorganic compounds, including oxides, nitrides, carbides, chalcogenides, and ceramics for many potential applications.[22–25] In recent years, there are some reports focused on mitigation of migration and agglomeration (coalescence) of Pt nanoparticles by coating oxides such as MnO_2[26] and SiO_2[27] or ionic liquid polymer (ILP)[28] on the catalyst surface. However, the activity of the catalysts coated by oxides and ILP was lower due to the poor conductivity of the coatings.

Herein, we have designed a microcapsule composite with multi-walled carbon nanotubes (MWCNTs) as microcapsule shell and TiO_2 as stuffing and then synthesized microcapsule Pt/MWCNTs-TiO_2 catalyst for PEMFCs by microwave-assisted polyol process (MAPP). Cyclic voltammetry and accelerated potential cycling tests (APCT) show that the microcapsule Pt/MWCNTs-TiO_2 catalyst presents remarkably high performance and substantially enhanced stability in comparison with Pt/C[29] and Pt/MWCNTs ones obtained by the same procedure.

In our previous work,[29,30] we have reported a method to strengthen the support region of the catalyst without blocking of active catalytic sites by *in situ* carbonization of glucose. Herein, we also used this method to treat further the as-prepared microcapsule Pt/MWCNTs-TiO_2 catalyst and obtained carbon riveted microcapsule Pt/MWCNTs-TiO_2 catalyst. Electrochemical measurements indicate that the carbon riveted microcapsule Pt/MWCNTs-TiO_2 catalyst has similar activity with that of Pt/C reported before.[29] Morever, APCT results show that the carbon riveted microcapsule Pt/MWCNTs-TiO_2 catalyst exhibits much higher stability than that of Pt/C[29] and that of carbon riveted Pt/TiO_2-C discussed in our previous work.[29]

2. Experimental

2.1. Materials preparation

2.1.1. Synthesis of Pt/MWCNTs and microcapsule Pt/MWCNTs-TiO_2. Hexachloroplatinic acid ($H_2PtCl_6 \cdot 6H_2O$) was purchased from Shanghai, China. Multi-walled carbon nanotubes (MWCNTs) (with outer diameter size of more than 50 nm and inner diameter size of about 30 nm) was obtained from Chengdu, China and 5 wt% Nafion solution was purchased from Dupont. Except where specified, all chemicals were of analytical grade and used as received. Anatase titanium dioxide (TiO_2) with particle size of 20 nm was obtained from Xuan Cheng Jing Rui New Material Co., Ltd, China. Pt/MWCNTs catalyst with the Pt loading of 20 wt% was synthesized by microwave-assisted polyol process (MAPP) in ethylene glycol (EG) solution with H_2PtCl_6 as a precursor.[30] Synthetic process in detail is as follows: 80 mg MWCNTs was dispersed into 60 mL EG and isopropyl alcohol (v/v = 4 : 1) in a beaker of 100 mL under ultrasonic treatment (from Shanghai, 53 KHz, 280W) for 1 h to form uniform ink, into which adding 2.7 mL of 0.038 mol L^{-1} H_2PtCl_6-EG solution with the subsequent mixing process for 3 h. The pH value of the slurry was adjusted by adding 1 mol L^{-1} NaOH-EG solution drop by drop to 12.00. Then the beaker was placed in the center of a microwave oven (2450 MHz, 800 W) and argon gas was feed into the ink for 15 min to remove oxygen for consecutive microwave heating 50 s to fix platinum nanoparticles on MWCNTs. The solution was allowed to cool down to room temperature by continuous agitation, and then 0.1 mol L^{-1} HNO_3 was added into the cooled mixture to adjust pH value of the solution to about 3–4. The mixture was kept stirring for 12 h and then the product was washed repeatedly with ultrapure water (Millipore, 18.2 MΩ cm). The 20 wt% microcapsule Pt/MWCNTs-TiO_2 catalysts was synthesized by the same procedures for preparing the Pt/MWCNTs catalyst, but the MWCNTs was replaced by the microcapsule composite of MWCNTs and anatase TiO_2. After the combination of MWCNTs with anatase TiO_2 was ultrasonicated for 2 h and agitated for 2 h, antatse TiO_2 entered the inside of MWCNTs because the inner diameter of MWCNTs was larger than the particle size of TiO_2. After TiO_2 entered the inside of the MWCNTs, the microcapsule composite of MWCNTs and TiO_2 was formed due to the interaction between MWCNTs and TiO_2. The obtained Pt/MWCNTs and microcapsule Pt/MWCNTs-TiO_2 catalysts were dried for 3 h at 80 °C and then stored in a vacuum vessel.

2.1.2. Preparation of carbon riveted microcapsule Pt/MWCNTs-TiO_2 catalyst. The carbon riveting process (CRP) of the microcapsule Pt/MWCNTs-TiO_2 catalyst was accomplished as follows. Firstly, 50 mg microcapsule Pt/MWCNTs-TiO_2 catalyst and 8.26 mg glucose ($C_6H_{12}O_6 \cdot H_2O$) were dispersed into 10 mL H_2O (Millipore, 18.2 MΩ·cm) in 50 mL beaker under ultrasonic treatment for 1 h to form uniform slurry. The slurry was first dried at 70 °C in a porcelain boat and then heated at 400 °C for 1 h in the tube furnace under argon. The product was cooled to room temperature in argon and then stored under vacuum.

2.1.3. Preparation of working electrode. The catalyst ink was prepared by ultrasonically dispersing 5.0 mg catalyst in 2.5 mL ethanol and the dispersion was then ultrasonicated for 20 min. The glassy carbon (GC) working electrode with 4 mm of diameter was polished with 0.05 μm alumina suspensions to a mirror finish before each experiment and served as an underlying substrate of the working electrode. A quantity of 10 μL of the dispersion was pipetted out on the top of the GC and onto which

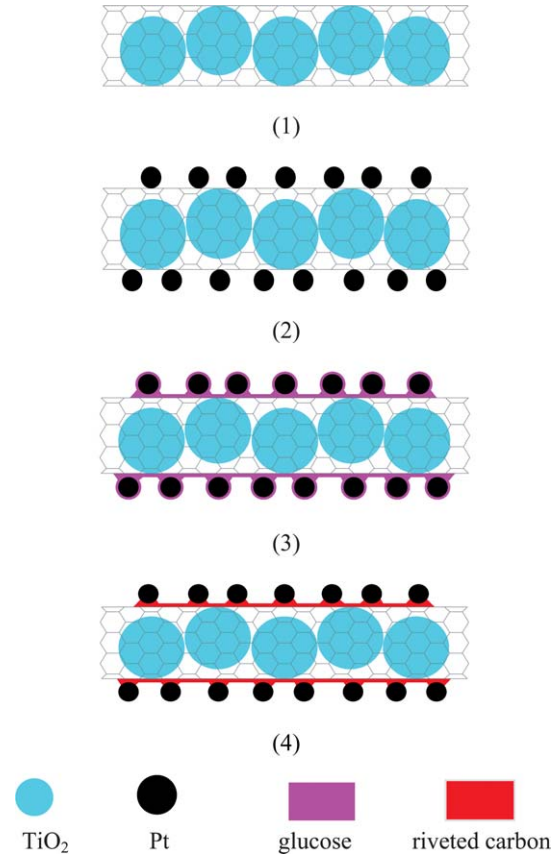

Scheme 1 Schematic diagram of carbon riveting process. (1) microcapsule support; (2) as-prepared microcapsule Pt/MWCNTs-TiO_2; (3) microcapsule Pt/MWCNTs-TiO_2 coated with glucose; (4) carbon riveted microcapsule Pt/MWCNTs-TiO_2.

5 μL of a dilute aqueous Nafion® solution (5 wt % solution in a mixture of lower aliphatic alcohols and DuPont water) was applied.

2.2. Electrochemical measurements

Electrochemical measurements were carried out in a conventional sealed three-electrode electrochemical cell at 25 °C, with the glassy carbon disk electrode made in the above mentioned procedure as the working electrode and a piece of Pt foil (1 cm^2) as the counter electrode. The Hg/Hg_2SO_4 reference electrode (−0.68 V relative to reversible hydrogen electrode, RHE) was placed in a separate chamber, which is located near the working electrode chamber through a Luggin capillary tube. All solutions were prepared with ultrapure water (Millipore, 18.2 MΩ cm). The solution of 0.5 mol L^{-1} H_2SO_4 was purged with ultrapure argon gas for nearly 30 min before starting the measurements. The cyclic voltammograms (CV) were recorded with CHI650D electrochemical analysis instrument within a potential range from −0.66 V to 0.49 V. In order to get rid of the possible effects caused by Nafion® film, the working electrode was treated by continuously cycling at 0.05 V s^{-1} until a stable response was obtained before the measurement curves were recorded. Fresh electrolyte solution was used for each electrochemical measurement to ensure reproducible results. All the potentials reported herein were *versus* the Hg/Hg_2SO_4 electrode.

The stability of the catalyst was evaluated by the accelerated potential cycling test (APCT) which was conducted within the potential range of −0.11–0.49 V. The electrochemical active specific surface area (ESA) of platinum was calculated with coulombic charges accumulated during hydrogen adsorption or desorption after correcting for the double-layer charging current from the CV:[31]

$$\mathrm{ESA} = \frac{Q_H}{0.21 \times M_{Pt}} \quad (1)$$

Where Q_H (mC) is the charge due to the hydrogen adsorption/desorption in the hydrogen region of the CVs, 0.21 mC cm^{-2} is the electrical charge associated with monolayer adsorption of hydrogen on Pt, and M_{Pt} is the loading of Pt metal on the working electrode.

2.3. Characterizations of physical properties

2.3.1. X-Ray diffraction (XRD). XRD analysis of nanomaterials was carried out with the D/max-RB diffractometer (made in Japan) using a Cu Ka X-ray source operating at 45 kV

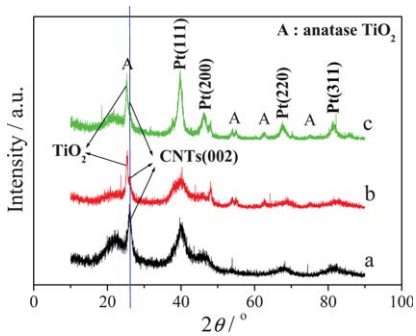

Fig. 1 XRD patterns of Pt/MWCNTs (a), microcapsule Pt/MWCNTs-TiO_2 (b), and carbon riveted microcapsule Pt/MWCNTs-TiO_2 (c) catalysts.

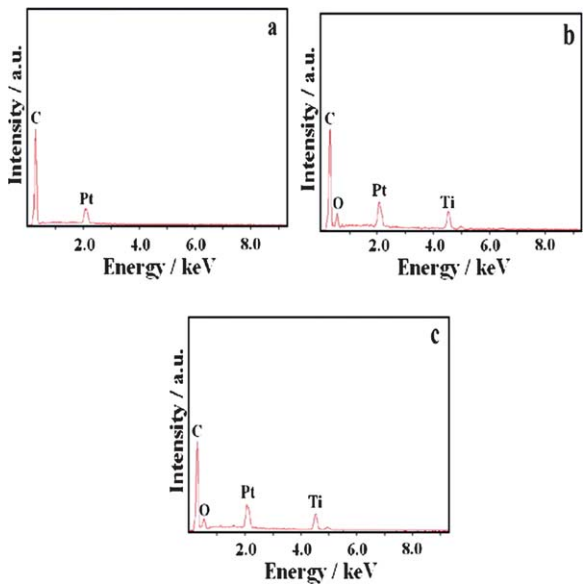

Fig. 2 EDAX patterns of Pt/MWCNTs (a), microcapsule Pt/MWCNTs-TiO_2 (b), and carbon riveted microcapsule Pt/MWCNTs-TiO_2 (c) catalysts.

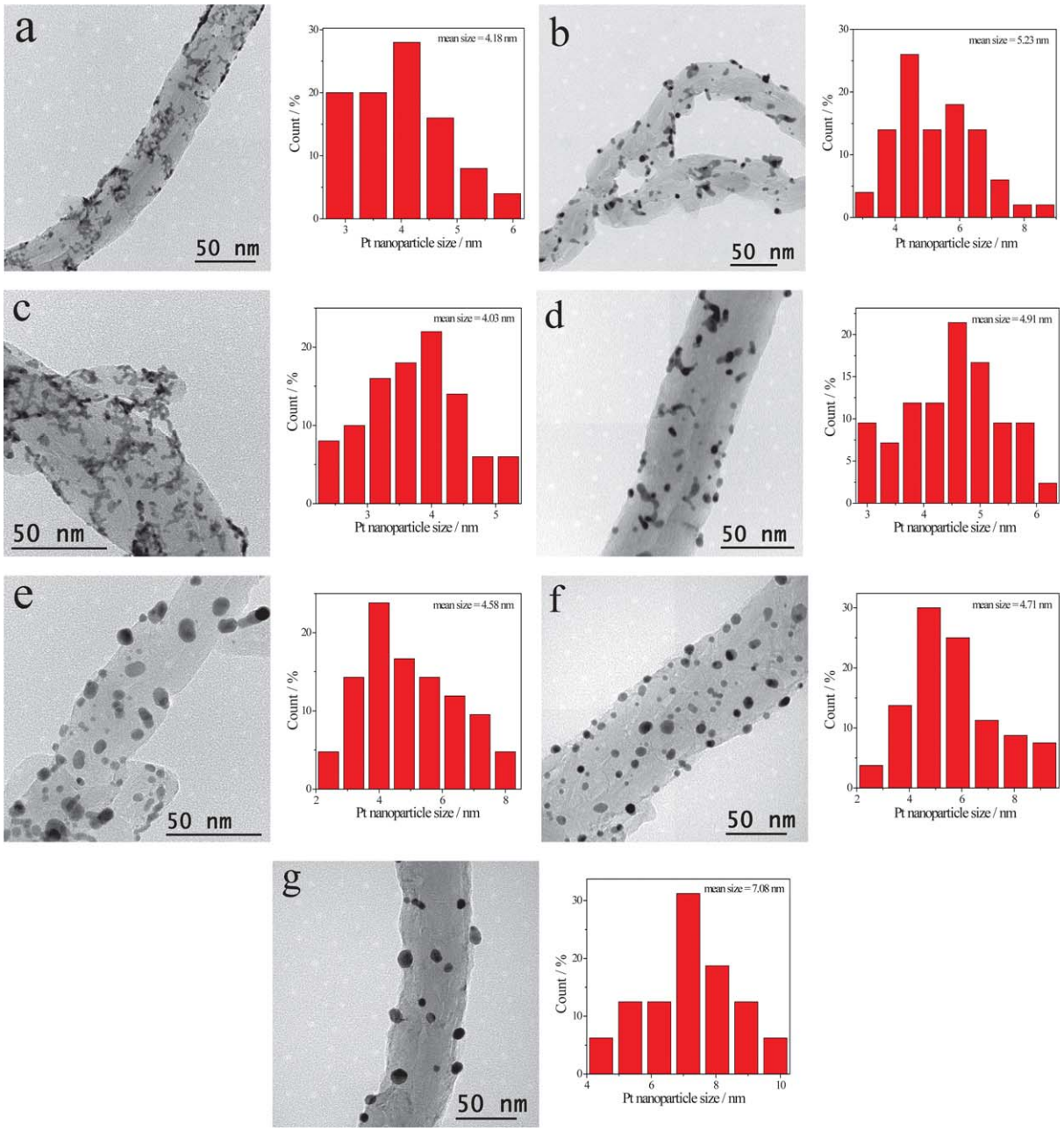

Fig. 3 TEM images and the size distributions of Pt/MWCNTs (a, b), microcapsule Pt/MWCNTs-TiO_2 (c, d) and carbon riveted microcapsule Pt/MWCNTs-TiO_2 (e, f, g) before (a, c, e) and after (b, d, f, g) APCT, (b, d, f) after 1000cycles APCT, (g) after 7500 cycles APCT.

and 100 mA, scanning at a rate of 4° min^{-1} with an angular resolution of 0.05° of the 2θ scan to get the XRD pattern.

2.3.2. Energy dispersive analysis of X-ray (EDAX). Hitachi-S-4700 analyzer was coupled to a scanning electron microscope (SEM, Hitachi Ltd. S-4700) for a rapid EDAX analysis of chemical composition. The samples were supported on the aluminum foil to eliminate the influence of the conductive carbon tape. The sample surface was impinged from the normal angle for 100 s by the X-ray incident electron beam with energies ranging from 3 to 30 keV.

2.3.3. Transmission electron microscopy (TEM) and scanning transmission electron microscopy (STEM). TEM and STEM for the catalyst samples were taken by a TECNAI G2 F30 field emission transmission electron microscope with a spatial resolution of 0.17 nm. Before taking the electron micrographs, the samples were finely ground and ultrasonically dispersed in isopropyl alcohol, and a drop of the resultant dispersion was deposited and dried on a standard copper grid coated with carbon film. The applied voltage was 300 kV.

2.3.4. X-Ray photoelectron spectroscopy (XPS). XPS analysis was carried out to determine the surface properties of the catalysts with a Physical Electronics PHI model 5700 instrument. The Al X-ray source was operated at 250 W and the take-off angle of the sample to analyzer was 45°. Survey spectra were collected at

Fig. 4 HAADF-STEM image of as-prepared microcapsule Pt/MWCNTs-TiO_2 catalyst.

a pass energy (PE) of 187.85 eV over a binding energy range from 0 eV to 1300 eV. High binding energy resolution multiplex data for the individual elements were collected at a PE of 29.55 eV. During all XPS experiments, the pressure inside the vacuum system was maintained at 1×10^{-9} Pa. Before analysis above, all the samples were dried under vacuum at 80 °C overnight.

2.3.5. Thermal gravimetric analysis/differential thermal analysis (TGA/DTA). TGA/DTA were carried out on Mettler-Toledo (TGA/SDTA851) thermal analyzer in air at the heating rate of 10° min^{-1} to obtain information on the decomposition and the burning properties of the catalyst. The temperature of the sample was varied from room temperature to 1000 °C.

2.3.6. Fourier transform infrared (FT-IR) spectra. FT-IR spectra of the MWCNTs was recorded on Nicolet Magna 550 FT-IR spectrometer. The samples for FT-IR studies were prepared by suspending approximately 6 mg of MWCNTs in 15 ml isopropyl alcohol by sonication for several minutes. One drop of this solution was sprayed onto silicon wafer and a uniform thin MWNTs film on the IR transparent silicon substrate was thus obtained. FT-IR studies were carried out in the range of 400–4000 cm^{-1} in the absorbance mode.

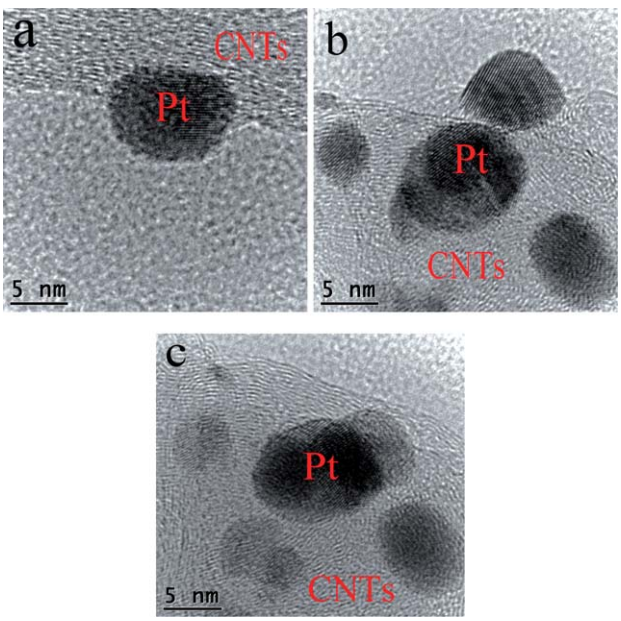

Fig. 5 High-resolution TEM images of as-prepared microcapsule Pt/MWCNTs-TiO_2 catalyst.

3. Results and discussion

Scheme 1 shows the four principal steps of carbon riveting process (CRP) as follows: (1) the microcapsule composite of MWCNTs with TiO_2, (2) the deposition of Pt nanoparticles onto the microcapsule support, (3) the coating of microcapsule Pt/MWCNTs-TiO_2 with glucose and finally (4) the *in situ* carbonization of glucose. The detailed experimental process was reported in our previous work.[30] This is an ideal diagram which indicates the contact of Pt with MWCNTs and TiO_2. Interestingly, Pt nanoparticles were designed to deposit more on the boundaries of the MWCNTs and TiO_2 in Scheme 1 (2) due to the fact that TiO_2 inside MWCNTs can increase the hydrophilicity of the contact sites of MWCNTs with TiO_2 and then augment deposition sites of Pt nanoparticles.

TGA/DTA measurements (see Fig. S1 in ESI for details†) show that the dominant weight loss of the sample occurs in the temperature range 400–600 °C corresponding to the removal of MWCNTs. Moreover, the small peak at about 350 °C on DTA pattern corresponds to the carbon layers on the surface of the catalyst formed during the CRP. The weight loss of the catalyst after the TGA-DTA experiment is in accordance with the theoretical value. FT-IR spectra (see Fig. S2 in ESI for details†) of the as grown MWCNTs shows dominant peaks at 3449, 2918, 1639, and 1418 cm^{-1} that are identified as C–OH, C–H, C═O, and C═O, respectively. These results indicate that non-treated MWCNTs are not prone to deposition of Pt.

XRD patterns of Pt/MWCNTs, microcapsule Pt/MWCNTs-TiO_2, and carbon riveted microcapsule Pt/MWCNTs-TiO_2 are shown in Fig. 1, respectively. Representative diffraction peaks of Pt [(111), (200), (220), and (311)] are distinctly observed in Pt/MWCNTs spectrum, which means that Pt forms the face-centered cubic (fcc) crystal structure. The presence of sharp peak at 26.1° in the XRD pattern of Pt-MWCNTs corresponds to CNTs (002), which is in accordance with the results by Cao and his co-workers.[32] Pt diffraction peaks are also presented in microcapsule Pt/MWCNTs-TiO_2 patterns, however, not clear, which is similar to the results reported by Wang and coworkers.[33] Pattern (c) that was assignable to carbon riveted microcapsule Pt/MWCNTs-TiO_2 catalyst also shows obvious diffraction peaks of Pt [(111), (200), (220), and (311)], illustrating that Pt nanoparticles have higher crystallinity after the CRP.

Fig. 2 shows the EDAX patterns of Pt/MWCNTs, microcapsule Pt/MWCNTs-TiO_2, and carbon riveted microcapsule Pt/MWCNTs-TiO_2 catalysts, respectively. It can be seen that the peaks of Pt element are distinct in all patterns, which further proves that Pt nanoparticles were deposited onto the supports in our experimental conditions. The Pt contents are 20.48 wt%, 20.43 wt%, and 19.94 wt% in Pt/MWCNTs, microcapsule Pt/MWCNTs-TiO_2, and carbon riveted microcapsule Pt/MWCNTs-TiO_2 catalysts, respectively, which are similar to the theoretical values. Moreover, Ti and O elements were also

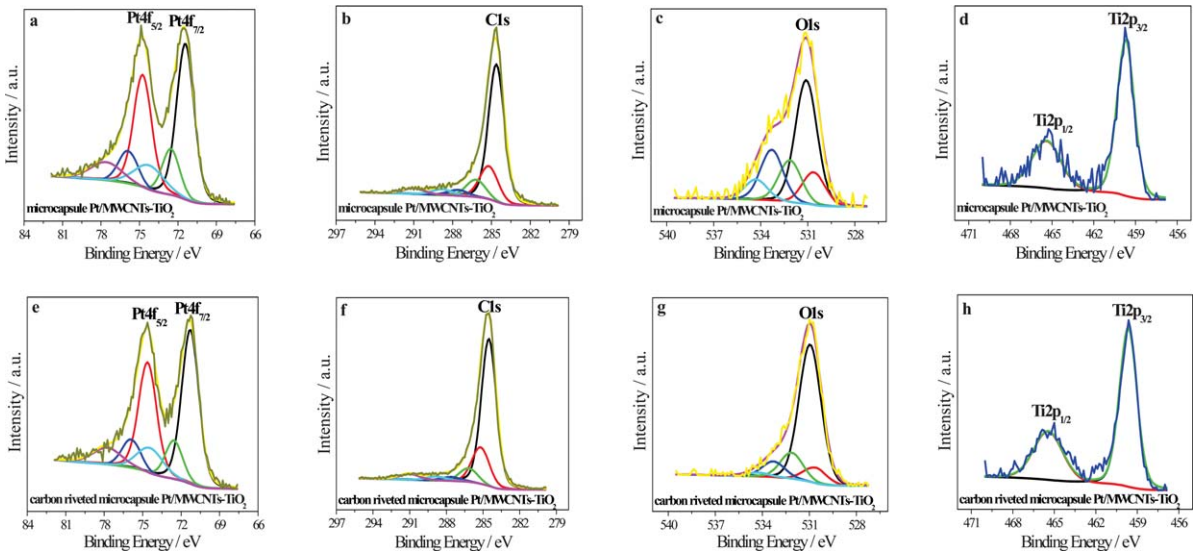

Fig. 6 Deconvoluted Pt 4f (a, e), C 1s (b, f), O1s (c, g), and Ti 2p (d, h) peaks from XPS analysis of microcapsule Pt/MWCNTs-TiO_2 (a, b, c, d) and carbon riveted microcapsule Pt/MWCNTs-TiO_2 (e, f, g, h) catalysts.

detected in both microcapsule Pt/MWCNTs-TiO_2, and carbon riveted microcapsule Pt/MWCNTs-TiO_2 catalysts.

TEM images with associated size distributions of Pt/MWCNTs, as-prepared microcapsule Pt/MWCNTs-TiO_2, and carbon riveted microcapsule Pt/MWCNTs-TiO_2 before and after APCT are shown in Fig. 3. It is clearly seen from Fig. 3a and Fig. 3c that the distribution of Pt nanoparticles of as-prepared microcapsule Pt/MWCNTs-TiO_2 is more uniform than that of Pt/MWCNTs, which is assignable to the fact that TiO_2 inside MWCNTs modifies the surface of MWCNTs and then augments the deposition sites of Pt nanoparticles. And the mean size of Pt nanoparticles of as-prepared microcapsule Pt/MWCNTs-TiO_2 is 0.15 nm smaller than that Pt/MWCNTs. Furthermore, after the CRP, the crystallite size of carbon riveted microcapsule Pt/MWCNTs-TiO_2 increases from 4.03 nm to 4.58 nm, showing that the process of Scheme 1 effectively anchors the crystallites and inhibits migration and agglomeration (coalescence) of the Pt nanoparticles.[30] With regard to the TEM micrographs after 1000 cycles APCT, it can be obviously seen that the crystallite sizes of Pt/MWCNTs, as-prepared microcapsule Pt/MWCNTs-TiO_2, and carbon riveted microcapsule Pt/MWCNTs-TiO_2 grow to 5.23 nm, 4.91 nm and 4.71 nm, increasing by 25.1%, 21.8%, and 2.8% in comparison with those before APCT, respectively. Furthermore, after 7500 cycles APCT, the crystallite size of carbon riveted microcapsule Pt/MWCNTs-TiO_2 increases to 7.08 nm, increasing by 54.59% in comparison with that of before APCT. And the results of TEM are in accordance to the results of electrochemical measurements discussed below. The high stability of microcapsule Pt/MWCNTs-TiO_2 catalyst is ascribed to two major factors: (1) the inherently excellent mechanical resistance and stability of anatase TiO_2 and MWCNTs in acidic and oxidative environments; (2) strong metal-support interaction (SMSI)[34–36] between Pt nanoparticles and microcapsule support. As to the ultrahigh stability of carbon riveted microcapsule Pt/MWCNTs-TiO_2 catalyst, besides the two factors mentioned above, there is one more critical reason that the riveted carbon formed during the CRP effectively anchors the crystallites and inhibits migration and agglomeration (coalescence) of the Pt nanoparticles during the APCT.

Fig. 4 represents the high angle annular dark field (HAADF) STEM image of as-prepared microcapsule Pt/MWCNTs-TiO_2, showing that Pt nanoparticles disperse uniformly on the MWCNTs surface. High-resolution TEM images of as-prepared microcapsule Pt/MWCNTs-TiO_2 catalyst is shown in Fig. 5. TiO_2 was not detected from the surface of MWCNTs in TEM,

Table 1 Results of the fits of the Pt 4f spectra, values given in % of total intensity

Sample	Pt(0) 71.48eV	Pt(II) 72.55 eV	Pt(IV) 74.27 eV
Microcapsule Pt/MWCNTs-TiO_2	64.25	18.7	17.05
Carbon riveted microcapsule Pt/MWCNTs-TiO_2	66.9	16.8	16.3

Table 2 Results of the fits of the C 1s spectra, values given in % of total intensity

Sample	sp^2-C 284.53 eV	sp^3-C 285.20 eV	C-OR 286.20 eV
Microcapsule Pt/MWCNTs-TiO_2	63.32	17.40	8.79
Carbon riveted microcapsule Pt/MWCNTs-TiO_2	66.44	18.73	6.73

Sample	C=O 287.60 eV	COOR 288.80 eV	Anti π bond 291.02 eV
Microcapsule Pt/MWCNTs-TiO_2	3.37	3.48	3.65
Carbon riveted microcapsule Pt/MWCNTs-TiO_2	2.25	2.31	3.54

high-resolution TEM and HAADF-STEM figures. Moreover, there was also no TiO_2 independent of MWCNTs in all carbon film field during the TEM test period. However, TiO_2 was detected obviously in EDAX, XRD, XPS, and TG patterns, respectively, illustrating adequately that TiO_2 enters the inside of MWCNTs and forms the microcapsule composite of MWCNTs with TiO_2. And the ratiocination mentioned above proves the design in Scheme 1.

Deconvoluted Pt 4f, C 1s, O 1s, and Ti 2p peaks from XPS analysis of as-prepared microcapsule Pt/MWCNTs-TiO_2 and carbon riveted microcapsule Pt/MWCNTs-TiO_2 catalysts are shown in Fig. 6. The curves fitting of Pt 4f, C 1s, and O 1s peaks of the X-ray photoelectron spectra for as-prepared microcapsule Pt/MWCNTs-TiO_2 and carbon riveted microcapsule Pt/MWCNTs-TiO_2 catalysts are in accordance with our previous work.[30] The binding energies of all components along with their relative intensities are provided in Table 1, Table 2, Table 3, and Table 4, respectively. Not surprisingly, the Pt(0) peaks of as-prepared microcapsule Pt/MWCNTs-TiO_2 and carbon riveted microcapsule Pt/MWCNTs-TiO_2 catalysts show a shift of the Pt 4f binding energy to the direction of higher energies by about 0.19 eV in comparison with that of Pt/MWCNTs (see Fig. S3 in ESI for details†), indicating further the strong metal-support interaction (SMSI) between Pt nanoparticles and TiO_2. Moreover, the content of Pt(0) increases by 2.65% accompanied with decreasing by 0.75% of Pt(IV), demonstrating that carbon riveted microcapsule Pt/MWCNTs-TiO_2 catalyst has higher stability relative to as-prepared microcapsule Pt/MWCNTs-TiO_2 due to more corrosion resistance of Pt(0).[13] As for the curve fitting of Ti 2p peak of the Ti X-ray photoelectron spectra before and after the CRP, it can be deconvoluted into two Gaussians centered at 459.66 eV and 465.44 eV, which correspond to perfect anatase TiO_2, illustrating that there was no crystal transformation of anatase TiO_2 and no anatase TiO_2 was reduced to metal Ti in the CRP. The XPS results of C 1s spectra show that the relative intensities of oxygen containing functional groups of carbon riveted microcapsule Pt/MWCNTs-TiO_2 catalyst are lower than those of as-prepared microcapsule Pt/MWCNTs-TiO_2, indicating that the carbonization of the glucose is thorough in the Scheme 1 process. Furthermore, it is also clearly seen in Table 2 that in carbon riveted microcapsule Pt/MWCNTs-TiO_2 catalyst the sp^3-C is 1.33% greater and the COOR group is 1.17% lower than that in as-prepared microcapsule Pt/MWCNTs-TiO_2 catalyst. This may be one of the critical reasons for the ultrahigh stability of the carbon riveted microcapsule Pt/MWCNTs-TiO_2 catalyst.

Cyclic voltammograms (CV) for Pt/MWCNTs, as-prepared microcapsule Pt/MWCNTs-TiO_2 and carbon riveted microcapsule Pt/MWCNTs-TiO_2 catalysts before and after APCT are carried out in 0.5 mol L^{-1} H_2SO_4 at 25 °C and shown in Fig. 7. Measurements of the hydrogen adsorption-desorption (HAD) integrals provide the electrochemically active specific surface areas (ESA) of Pt nanoparticles. The variations of the ESA values calculated from the hydrogen desorption integrals with cycle number during the APCT are shown in Fig. 8. Standard HAD regions of Pt are presented on microcapsule Pt/MWCNTs-TiO_2 catalyst and its ESA before APCT reach as high as 85.42 m^2 g_{Pt}^{-1} that is higher than 81.54 m^2 g_{Pt}^{-1} of Pt/C by the same procedure,[27] which is attributed to the uniform dispersion of Pt nanoparticles on the microcapsule support by the MAPP. Pt nanoparticles are more easily to be deposited on TiO_2 surface than on MWCNTs because of the stronger hydrophilicity of TiO_2 than MWCNTs. Then if there was TiO_2 independent of MWCNTs, the activity of as-prepared microcapsule Pt/MWCNTs-TiO_2 catalyst would be lower than Pt/MWCNTs due to less Pt nanoparticles on the MWCNTs. And the high activity of as-prepared microcapsule Pt/MWCNTs-TiO_2 catalyst indicates further that there was no TiO_2 independent of MWCNTs. The analysis is consistent with the results of TEM, HRTEM and HAADF-STEM figures, confirming further the design in Scheme 1. Moreover, due to bigger mean size and irregular dispersion of Pt nanoparticles that are displayed in Fig. 3, ESA of Pt/MWCNTs is only 78.29 m^2 g_{Pt}^{-1}. As for the carbon riveted microcapsule Pt/MWCNTs-TiO_2, its ESA before APCT is 81.32 m^2 g_{Pt}^{-1}, which is very close to those of as-prepared microcapsule Pt/MWCNTs-TiO_2 and Pt/C, demonstrating that the mean size of Pt nanoparticles doesn't increase evidently in the CRP. From Fig. 8, it can be clearly seen that ESA of Pt/MWCNTs reduces 32% after 1000 cycles APCT. However, ESA of as-prepared microcapsule Pt/MWCNTs-TiO_2 and carbon riveted microcapsule Pt/MWCNTs-TiO_2 catalysts decrease by 28% and 4% after the same tests, showing that the carbon riveted microcapsule Pt/MWCNTs-TiO_2 catalyst has much higher stability than microcapsule Pt/MWCNTs-TiO_2 with similar activity. Furthermore, ESA of carbon riveted microcapsule Pt/MWCNTs-TiO_2 catalyst reduces 21% after 3000 cycles APCT and reduces 47% after 7500 cycles APCT. However, according to our previous work,[27] ESA of Pt/C and carbon riveted Pt/TiO_2-C decreases by 49% and 22% after 1000 cycles APCT,

Table 3 Results of the fits of the O 1s spectra, values given in % of total intensity

Sample	530.62 eV	531.10 eV	532.14 eV
Microcapsule Pt/MWCNTs-TiO_2	12.32	45.26	15.70
Carbon riveted microcapsule Pt/MWCNTs-TiO_2	8.06	68.61	13.33

Sample	533.30 eV	534.30 eV
Microcapsule Pt/MWCNTs-TiO_2	19.13	7.60
Carbon riveted microcapsule Pt/MWCNTs-TiO_2	8.06	1.94

Table 4 Results of the fits of the Ti 2p spectra, values given in % of total intensity

Sample	459.66 eV	465.44 eV
Microcapsule Pt/MWCNTs-TiO_2	66.67	33.33
Carbon riveted microcapsule Pt/MWCNTs-TiO_2	66.69	33.31

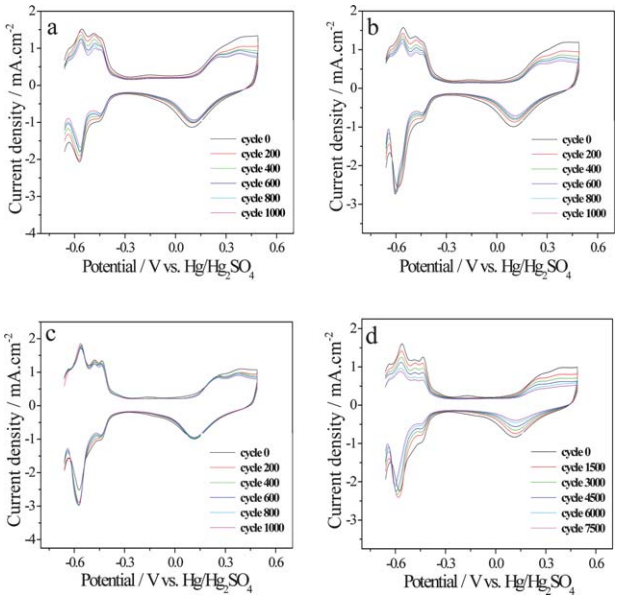

Fig. 7 CV in 0.5 mol L^{-1} H_2SO_4 for Pt/MWCNTs (a), as-prepared microcapsule Pt/MWCNTs-TiO_2 (b) and carbon riveted microcapsule Pt/MWCNTs-TiO_2 (c, d) catalysts during the APCT.

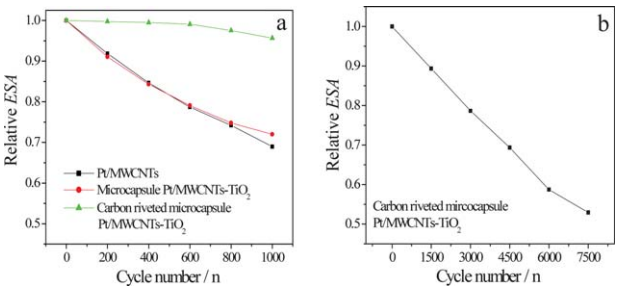

Fig. 8 Relationship of ESA and cycle number for Pt/MWCNTs (a), as-prepared microcapsule Pt/MWCNTs-TiO_2 (a) and carbon riveted microcapsule Pt/MWCNTs-TiO_2 (a, b) catalysts during the APCT. Scanning rate: 50 mV s^{-1}; test temperature: 25 °C.

respectively.[29] The results show that the carbon riveted microcapsule Pt/MWCNTs-TiO_2 catalyst possesses 7.5-times as high stability as that of Pt/C[29] and has 3-times as long life-span as that of carbon riveted Pt/TiO_2-C.[29]

4. Conclusions

In conclusion, we have synthesized Pt/MWCNTs and microcapsule Pt/MWCNTs-TiO_2 by microwave-assisted polyol process. Microcapsule Pt/MWCNTs-TiO_2 catalyst presents higher activity compared to Pt/C and Pt/MWCNTs by the same procedure. Furthermore, we have designed and synthesized a carbon riveted microcapsule Pt/MWCNTs-TiO_2 catalyst based on *in situ* carbonization of the glucose. The measurement results show that the carbon riveted microcapsule Pt/MWCNTs-TiO_2 catalyst with similar activity to Pt/C and microcapsule Pt/MWCNTs-TiO_2 possesses 7.5-times as high stability as that of Pt/C and has 3-times as long life-span as that of carbon riveted Pt/TiO_2-C reported in our previous work. The significantly enhanced stability for carbon riveted microcapsule Pt/MWCNTs-TiO_2 catalyst is attributed to three critical reasons: (1) the inherently excellent mechanical resistance and stability of anatase TiO_2 and MWCNTs in acidic and oxidative environments; (2) strong metal-support interaction between Pt nanoparticles and the microcapsule support; (3) the anchoring effect of the carbon layers formed during the carbon riveting process. Furthermore, the increase of Pt(0) composition during the carbon riveting process is also propitious to the improvement of the catalyst stability. Full tests of these supported catalysts in single fuel cells are still in process. Considering the importance of the stability of the catalysts in fuel cell environments, carbon riveted microcapsule Pt/MWCNTs-TiO_2 catalyst is a promising catalyst not only for proton exchange membrane fuel cells, but also for higher temperature fuel cells where the problem of catalyst growth is more serious.

Acknowledgements

This research is financially supported by the National Natural Science Foundation of China (Grant No. 20606007), the Scientific Research Foundation for the Returned Overseas Chinese Scholars, State Education Ministry (2008), and Scientific Research Foundation for Returned Scholars of Heilongjiang Province of China (LC08C33).

References

1 C. Koenigsmann and S. S. Wong, *Energy Environ. Sci.*, 2011, **4**, 1161.
2 F. Jaouen, E. Proietti, M. Lefevre, R. Chenitz, J.-P. Dodelet, G. Wu, H. T. Chung, C. M. Johnston and P. Zelenay, *Energy Environ. Sci.*, 2011, **4**, 114–130.
3 E. Reddington, A. Sapienza, B. Gurau, R. Viswanathan, S. Sarangapani, E. S. Smotkin and T. E. Mallouk, *Science*, 1998, **280**, 1735–1737.
4 S. S. Zhang, X. Z. Yuan, J. N. C. Hin, H. J. Wang, K. A. Friedrich and M. Schulze, *J. Power Sources*, 2009, **194**, 588–600.
5 J. F. Wu, X. Z. Yuan, J. J. Martin, H. J. Wang, J. J. Zhang, J. Shen, S. H. Wu and W. Merida, *J. Power Sources*, 2008, **184**, 104–119.
6 Y. K. Zhou, K. Neyerlin, T. S. Olson, S. Pylypenko, J. Bult, H. N. Dinh, T. Gennett, Z. P. Shao and R. O'Hayre, *Energy Environ. Sci.*, 2010, **3**, 1437–1446.
7 D. Wang, S. Lu and S. P. Jiang, *Chem. Commun.*, 2010, **46**, 2058–2060.
8 S.-I. Choi, R. Choi, S. W. Han and J. T. Park, *Chem. Commun.*, 2010, **46**, 4950–4952.
9 Z.-B. Wang, G.-P. Yin and Y.-G. Lin, *J. Power Sources*, 2007, **170**, 242–250.
10 M. Carmo, M. Linardi and J. G. Rocha Poco, *Int. J. Hydrogen Energy*, 2008, **33**, 6289–6297.
11 K. Miyatake, T. Omata, D. A. Tryk, H. Uchida and M. Watanabe, *J. Phys. Chem. C*, 2009, **113**, 7772–7778.
12 W. Li and A. M. Lane, *Electrochim. Acta*, 2010, **55**, 6926–6931.
13 W. Li and A. M. Lane, *Electrochem. Commun.*, 2009, **11**, 1187–1190.
14 Z.-B. Wang, P.-J. Zuo, X.-P. Wang, J. Lou, B.-Q. Yang and G.-P. Yin, *J. Power Sources*, 2008, **184**, 245–250.
15 W. Zhang, J. Chen, G. F. Swiegers, Z.-F. Ma and G. G. Wallace, *Nanoscale*, 2010, **2**, 282–286.
16 F. Hasche, M. Oezaslan and P. Strasser, *Phys. Chem. Chem. Phys.*, 2010, **12**, 15251–15258.
17 Y. Y. Shao, G. P. Yin, Y. Z. Gao and P. F. Shi, *J. Electrochem. Soc.*, 2006, **153**, A1093–A1097.
18 X. Wang, W. Z. Li, Z. W. Chen, M. Waje and Y. S. Yan, *J. Power Sources*, 2006, **158**, 154–159.
19 X. Liu, J. Chen, G. Liu, L. Zhang, H. Zhang and B. Yi, *J. Power Sources*, 2010, **195**, 4098–4103.
20 A. Bauer, C. Song, A. Ignaszak, R. Hui, J. Zhang, L. Chevallier, D. Jones and J. Rozière, *Electrochim. Acta*, 2010, **55**, 8365–8370.

21 S. L. Gojkovic, B. M. Babic, V. R. Radmilovic and N. V. Krstajic, *J. Electroanal. Chem.*, 2010, **639**, 161–166.
22 D. Eder, *Chem. Rev.*, 2010, **110**, 1348–1385.
23 F. Stoffelbach, A. Aqil, C. Jerome, R. Jerome and C. Detrembleur, *Chem. Commun.*, 2005, 4532–4533.
24 X. Xie and L. Gao, *Carbon*, 2007, **45**, 2365–2373.
25 J. Sun, M. Iwasa, L. Gao and Q. Zhang, *Carbon*, 2004, **42**, 895–899.
26 C. Zhou, F. Peng, H. Wang, H. Yu, C. Peng and J. Yang, *Electrochem. Commun.*, 2010, **12**, 1210–1213.
27 S. Takenaka, H. Matsumori, T. Arike, H. Matsune and M. Kishida, *Top. Catal.*, 2009, **52**, 731–738.
28 B. Wu, D. Hu, Y. Yu, Y. Kuang, X. Zhang and J. Chen, *Chem. Commun.*, 2010, **46**, 7954–7956.
29 Z.-Z. Jiang, Z.-B. Wang, Y.-Y. Chu, D.-M. Gu and G.-P. Yin, *Energy Environ. Sci.*, 2011, **4**, 728–735.
30 Z.-Z. Jiang, Z.-B. Wang, D.-M. Gu and E. S. Smotkin, *Chem. Commun.*, 2010, **46**, 6998–7000.
31 Y. Xing, *J. Phys. Chem. B*, 2004, **108**, 19255–19259.
32 A. Cao, C. Xu, J. Liang, D. Wu and B. Wei, *Chem. Phys. Lett.*, 2001, **344**, 13–17.
33 X. Wang, J. C. Yu, H. Y. Yip, L. Wu, P. K. Wong and S. Y. Lai, *Chem.–Eur. J.*, 2005, **11**, 2997–3004.
34 D. R. Rolison, *Science*, 2003, **299**, 1698–1701.
35 A. Dauscher, L. Hilaire, F. Le Normand, W. Müller, G. Maire and A. Vasquez, *Surf. Interface Anal.*, 1990, **16**, 341–346.
36 F. Pesty, H.-P. Steinrück and T. E. Madey, *Surf. Sci.*, 1995, **339**, 83–95.

